Review of Scientific Instruments

Detection of single analyte and environmental samples with silicon nitride nanopores: Antarctic dirt particulates and DNA in artificial seawater

Cite as: Rev. Sci. Instrum. **91**, 031301 (2020); https://doi.org/10.1063/1.5138210
Submitted: 14 November 2019 . Accepted: 18 February 2020 . Published Online: 25 March 2020

David J. Niedzwiecki, Yung-Chien Chou, Zehui Xia, Federico Thei, and Marija Drndić

COLLECTIONS

This paper was selected as Featured

View Online Export Citation CrossMark

© 2020 Author(s).

Review of Scientific Instruments ARTICLE scitation.org/journal/rsi

Detection of single analyte and environmental samples with silicon nitride nanopores: Antarctic dirt particulates and DNA in artificial seawater

Cite as: Rev. Sci. Instrum. 91, 031301 (2020); doi: 10.1063/1.5138210
Submitted: 14 November 2019 • Accepted: 18 February 2020 •
Published Online: 25 March 2020

View Online Export Citation CrossMark

David J. Niedzwiecki,[1,a)] Yung-Chien Chou,[2] Zehui Xia,[1] Federico Thei,[3] and Marija Drndić[2,a)]

AFFILIATIONS

[1]Goeppert LLC, Pennovation Works, 3401 Grays Ferry Avenue, Philadelphia, Pennsylvania 19146, USA
[2]Department of Physics and Astronomy, David Rittenhouse Laboratory, University of Pennsylvania, 209 S. 33rd Street, Philadelphia, Pennsylvania 19103, USA
[3]Elements, SRL, Viale G. Marconi 438, Cesena 47521, Italy

[a)]**Authors to whom correspondence should be addressed:** dn@gppert.com and drndic@physics.upenn.edu

ABSTRACT

Nanopore sensing is a powerful tool for the detection of biomolecules. Solid-state nanopores act as single-molecule sensors that can function in harsh conditions. Their resilient nature makes them attractive candidates for taking this technology into the field to measure environmental samples for life detection in space and water quality monitoring. Here, we discuss the fabrication of silicon nitride pores from ~1.6 to 20 nm in diameter in 20-nm-thick silicon nitride membranes suspended on glass chips and their performance. We detect pure laboratory samples containing a single analyte including DNA, BSA, microRNA, TAT, and poly-D-lys-hydrobromide. We also measured an environmental (mixed-analyte) sample, containing Antarctic dirt provided by NASA Ames. For DNA measurements, in addition to using KCl and NaCl solutions, we used the artificial (synthetic) seawater, which is a mixture of different salts mimicking the composition of natural seawater. These samples were spiked with double-stranded DNA (dsDNA) fragments at different concentrations to establish the limits of nanopore sensitivity in candidate environment conditions. Nanopore chips were cleaned and reused for successive measurements. A stand-alone, 1-MHz-bandwidth Chimera amplifier was used to determine the DNA concentration in artificial seawater that we can detect in a practical time scale of a few minutes. We also designed and developed a new compact nanopore reader, a portable read-out device with miniaturized fluidic cells, which can obtain translocation data at bandwidths up to 100 kHz. Using this new instrument, we record translocations of 400 bp, 1000 bp, and 15000 bp dsDNA fragments and show discrimination by analysis of current amplitude and event duration histograms.

Published under license by AIP Publishing. https://doi.org/10.1063/1.5138210

I. INTRODUCTION

Nanopore-based[1,2] DNA and biomolecule analysis is a single-molecule technique, promising a range of electrical-based analyses orders of magnitude faster and more economical than many current methods.[2–40] The basic concept involves using an applied voltage to electrophoretically drive DNA or other molecules through a narrow pore, which separates chambers of electrolyte solution. This voltage also drives a flow of electrolyte ions through the nanopore, measured as an ionic current. When molecules pass through the pore, they modify the flow of ions, and structural information can be extracted by the analysis of the fluctuations of the resulting current.

Nanopores were first envisioned in the early 1990s in the context of protein pores (alpha-hemolysin) by Kasianowicz *et al.* who analyzed individual polynucleotide molecules.[1,2] Subsequently, nanopores have also been used for the detection of a wide range of organic and inorganic molecules and particles from anthrax toxin[41] and microRNA[42] to gold nanoparticles.[43] The general idea to detect particles using holes as partitions between electrolyte solutions originated even earlier from a patent by Coulter[44] in the 1950s for counting and sizing of particles by running them through single

holes of desired sizes, separating two electrolyte solutions, used today as a technology for blood cell counting. Both biological and solid-state nanopore platform development resulted from efforts searching for advanced technologies to improve the quality and efficiency of DNA sequencing, specifically for high-quality longer reads at low cost.

Beyond DNA sequencing as one of the highest profile applications of nanopores, for many applications from medicine to agriculture and food safety, there is strong demand for advanced analysis systems, in general, which are single molecule, massively parallel, high throughput, and real time. Commercial technologies based on biological nanopores have recently emerged and have been used for nanopore-based DNA sequencing and assembly of a human genome.[33] There are other opportunities for nanopores for low-abundance biomarker sensing for the diagnosis of illnesses and other important uses of nanopores for filtration, separation, and detection.[34] Benner[45] proposed nanopore-based instruments that could be used to detect life in ocean worlds beyond the Earth,[46,47] and biological nanopores for DNA sequencing have been tested on environmental samples at field sites such as the Atacama Desert, Antarctic Dry Valley, and Mars analog samples, and on the International Space Station.[48–51] Bywaters *et al.*[52] recently identified solid-state nanopores as attractive alternatives to biological pores for robust nanopore platforms that could retain their functionality for long duration space missions. The following has to be satisfied: first, the nanopore sensor should have excellent signal-to-noise characteristics to be able to detect and resolve small molecules quickly. In addition, and particularly for NASA space needs, the sensor has to be robust: it has to be able to survive a space flight and satisfy the stringent environmental and other requirements imposed for this specific application, such as planetary protection. Other requirements, such as autonomous operation, may also be required for space missions.

Nanopore readers could complement other technologies envisioned for field and space missions, for example, optical, Raman, and mass spectroscopies, to determine the sample's physical and chemical properties. Nanopores can characterize polymers in a sequential manner, reading out their charge and/or size variation. This complements mass spectroscopy, which could give precise data of the polymer constituent parts, yet may not maintain information regarding the sequence of those parts along the polymer. Additionally, nanopores could be used for precise sample filtration before analyses by other means.

In this paper, we present results from silicon nitride nanopore-based testing of two kinds of samples, pure and environmental samples, including DNA, BSA, microRNA, TAT, poly-D-lys-hydrobromide in KCl solutions, particulates from Antarctic dirt from the Linnaeus Terrace, Antarctic Dry Valleys, provided by NASA Ames and DNA molecules in artificial (synthetic) seawater samples. Synthetic seawater[53,54] is a mixture of many different salts mimicking the composition of natural seawater. We use the term "pure sample" here to indicate a laboratory sample with a single analyte so that we were only measuring one analyte at a time. This is in contrast to the environmental sample presented by the Antarctic dirt dissolved in distilled water, which contains a mixture of analytes.

Silicon nitride is an excellent nanopore material candidate because it has NASA space flight heritage and it was exposed to previous tests for required performance, durability, and resilience to harsh conditions.[55–58] Nanopore materials and membranes must be capable of withstanding operation in space and planetary environments, including the expected pressures, radiation levels, launch and impact stresses, and range of survival and operational temperatures. In addition, sensors must reduce mass, power, and volume, and instrument components without loss of scientific capability. Nanopore readers are ideal candidates for these applications because they can detect single molecules one by one and because their spatial and temporal resolution and sensitivity can be tailored by controlling the nanopore material, diameter, and thickness, as well as tailoring the surrounding sensing electronics including the amplifier bandwidth and its input-referred noise.

We measured samples using a stand-alone, higher-bandwidth, 1-MHz, Chimera amplifier setup[28,30] and a new portable hand-held "nanopore reader" that we have developed in this work toward field use. The nanopore reader, fluidic cell, and nanopore chip are hand-held. Purification of samples from environment would require further miniaturization. The portable reader was integrated with optimized SiN_x-on-glass chips for microliter sample volumes and can be of broad use, facilitating a wide range of nanopore-based applications. The nanopore reader is only a few centimeters in size (101 × 44 × 18 mm^3 and 140 g), allowing easy testing of environmental samples at maximum bandwidth up to 100 kHz, sufficient to detect and analyze most small molecules. The setup features an integrated fluidic cell housing noise-optimized, millimeter size nanopore chips. Solid-state nanopores here act as single-molecule sensors that can function in a variety of harsh conditions, such as pH and temperature. The resilient nature of solid-state nanopores makes them attractive for taking this technology into the field to measure environmental samples for life detection applications and water quality monitoring. The portable nanopore reader development here was partly motivated by sensor development needs for space research, such as in search for extraterrestrial life forms in recently discovered distant ocean worlds on moons of Jupiter and Saturn (Europa, Titan, Enceladus, and others).[46]

Motivated by these general goals, we show that 20-nm-thick silicon nitride nanopores are robust enough for measurements of simple analogs of the relevant environmental samples. Specifically, we used artificial (synthetic) seawater samples containing double-stranded DNA (dsDNA) fragments, presenting one of the simplest analogs toward the follow-up studies of more complex environmental ocean water samples. We tested samples containing DNA fragments of different lengths, 400 base pairs (bp), 1000 bp, 1500 bp, and 15 000 bp at a range of concentrations (0–100 nM). We show the discrimination of DNA fragments by the analysis of current signal and event duration magnitudes using an open source analysis software. The excellent sensitivity of the portable platform is also made possible by the characteristics of the SiN_x pores and chips made compatible with the nanopore reader's fluidic cell. Specifically, we use relatively thin yet robust SiN_x pores, drilled in 20-nm-thick, free-standing, low-stress SiN_x membranes, to lower the nanopore resistance and maximize the ion current signal for a fixed voltage applied across the pore (up to 1 V). Importantly, we suspend the SiN_x membranes on low-capacitance fused-silica (glass) chips, thus minimizing the overall chip capacitance and the capacitive noise, particularly at the higher frequencies. Ionic current measurements were also performed with a larger, stand-alone, 1 MHz, Chimera amplifier setup. The smallest concentration of DNA in synthetic seawater that we tested is 1 nM, corresponding

Published under license by AIP Publishing

to the detection of ~40 dsDNA molecules/min. The pores can also be cleaned and reused.

II. EXPERIMENTAL DETAILS

We first describe the properties of the glass chips with SiN_x nanopores, designed to fit the reader's fluidic cell (Figs. 1 and 2), followed by a description of the measurement setups: the new nanopore reader (fluidic cell and amplifier) in Fig. 3 and the 1-MHz-bandwidth Chimera setup for higher-bandwidth measurements in a laboratory setting (Fig. 4). Translocation measurement results on positively and negatively charged molecules (BSA, microRNA, TAT, and poly-D-lys-hydrobromide) are discussed in Fig. 5. These analytes were chosen to span a range of sizes and charges. Additionally, we present nanopore detection of particulates from Antarctic dirt in Fig. 6 and DNA fragments from 100 bp to 15 000 bp long and in artificial (synthetic) seawater samples and in 1 M KCl in Figs. 7 and 8.

The schematic of the experimental setup to measure molecular translocation through nanopores is shown in Fig. 1(a). When a bias voltage is applied across two electrolyte solution chambers separated by a dielectric membrane containing a nanopore, charged molecules are driven through the nanopore, blocking the baseline ionic current. This current block can be measured by a sensitive amplifier. To make small-diameter and thin pores within low-capacitance membranes, we fabricate fused-silica (glass) substrates [Figs. 1(a)–1(d)] instead of using a conventional silicon substrate to suspend the silicon nitride membrane.[28,32]

A. Fused-silica (glass) chips with suspended SiN_x membranes

The fabricated fused-silica (glass) substrates are shown in Figs. 1(b)–1(d). These chips are 300 μm thick and designed to reduce the chip capacitance below ~2 pF, thus lowering measurement noise at higher bandwidths as shown by Balan *et al.*[30,31] The chips can be circular or square and feature in their center a circular SiN_x membrane ~50 μm in diameter and 20 nm or 100 nm thick [Figs. 1(b) and 1(c)]. The low-stress silicon nitride membranes were grown and deposited by low-pressure chemical vapor deposition (LPCVD) using the same procedure as shown in previous studies.[1,2,34] Their stoichiometry was previously calibrated[59] using electron energy loss spectroscopy (EELS) showing an approximate ratio of Si:N ~ 3:4. Membrane thinning to below 10 nm can be further performed by reactive ion etching[42,60] to reduce the pore resistance. Replacing the typical silicon substrates by fused silica (glass) lowered the chip capacitance from the typical ~10–50 pF to the sub-pF to single pF range.[30,31]

B. Silicon nitride nanopores from ~1.8 nm to 20 nm in diameter

Figure 2 shows TEM images of fabricated SiN_x nanopores on glass chips, in order of increasing diameters for membrane thickness t = 20 nm [Figs. 2(a)–2(g)] and t = 100 nm [Fig. 2(h)]. White circles in Figs. 2(a)–2(h) outline the area of the pore and are used to determine the diameter prior to ionic measurements, together with intensity profiles across the pore, shown for pores in Figs. 2(e)–2(h). Figure 2(i) shows an array of nine pores with diameters from d = 2.0–10.2 nm within an ~60 × 60 nm^2 membrane area, illustrating a high density of pores that can be made. Pores were drilled with a 200 keV focused electron beam in a JEOL 2010F transmission electron microscope[28,61] within ~1 min., allowing a large number of pores to be made on a single chip in a short time. The TEM holder currently accommodates one chip at a time limiting the fabrication to about four to six nanopore chips/h. There are other methods of pore fabrication, such as electroporation[62] and laser illumination,[63–66] which may possibly prove to be higher throughput (see also, for example, a nanofabrication review[34] by Danda, Current Opinion in Biotechnology, 2019). Pores are drilled with

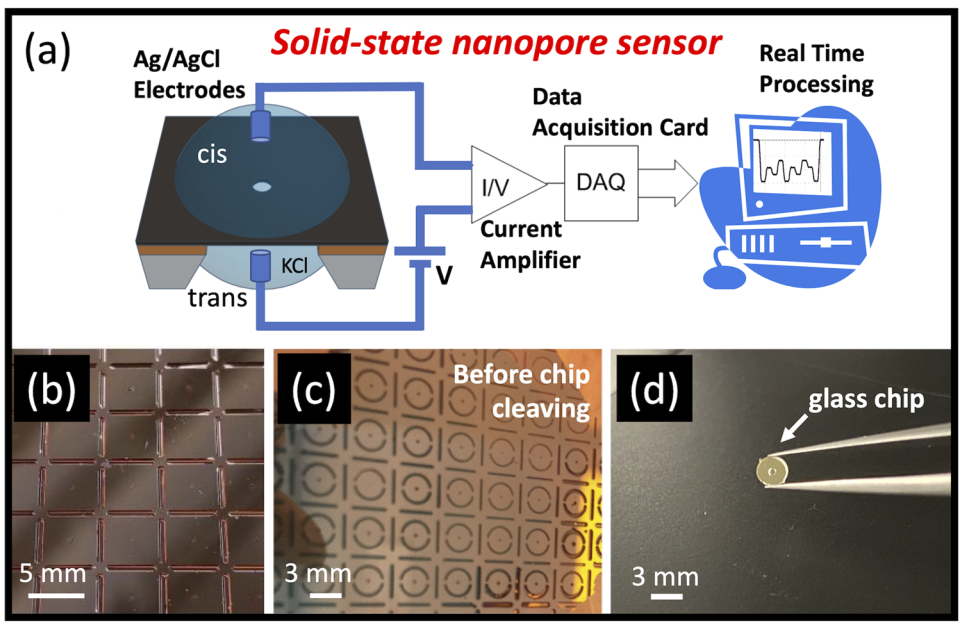

FIG. 1. (a) Schematic of a solid-state nanopore sensor composed of the membrane chip with a nanopore through it, connected to an amplifier with a fast data acquisition card. A voltage applied to the solution bath drives charged molecules through the nanopore. Ag/AgCl electrodes on both sides of the membrane are immersed in solution and used to record the ionic current signal over time. (b) and (c) Optical images of square 5 mm by 5 mm glass chips (b) and circular 3-mm-diameter glass chips (c) as part of the larger 4-in.-wafer during wafer-scale processing. (d) Photograph of an individual chip held by tweezers after cleaving from the substrate and before insertion into the fluidic cell. An optical micrograph of the circular SiN_x window in the middle of this chip is shown in Fig. 5(c). These chips are also compatible with standard TEM holders and TEM characterization and drilling.

Published under license by AIP Publishing

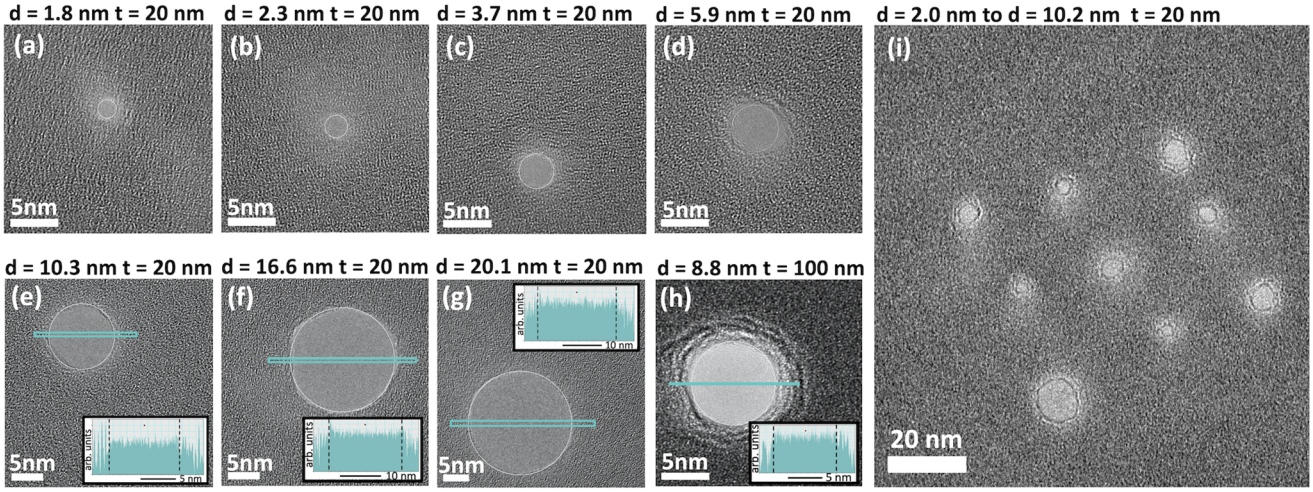

FIG. 2. Transmission electron microscope images of SiN_x nanopores fabricated on glass chips, with diameters d_{TEM} = 1.8 nm–20.1 nm in 20-nm-thick [(a)–(g) and (i)] and (h) 100-nm-thick SiN_x membranes; (i) shows an array of nine pores from d_{TEM} = 2.0–10.2 nm within an ~60 × 60 nm^2 membrane area. White circles in (a)–(h) outline the area of the pore and are used to determine the diameter, together with intensity profiles across the pore [as illustrated for pores in (e)–(h)]. Scale bars are 5 nm for (a)–(h) and 20 nm for (i).

diameter precision of about 0.3 nm for ~10-nm-diameter pores and ~0.1 nm for smaller diameter pores. The electron beam is focused to cross sectional size of less than 0.1 nm. Translocation measurement data in this work are reported from the 20-nm-thick membrane chips.

Nanopore diameter measurement error from TEM images and TEM-signal profile in Fig. 2 is ±0.1 nm. Before translocation measurements, we cleaned the pore to optimize pore wetting and performance. First, we cleaned the pore in 80 °C piranha for 5 min, followed by repeated rinsing in deionized (DI) water and drying it

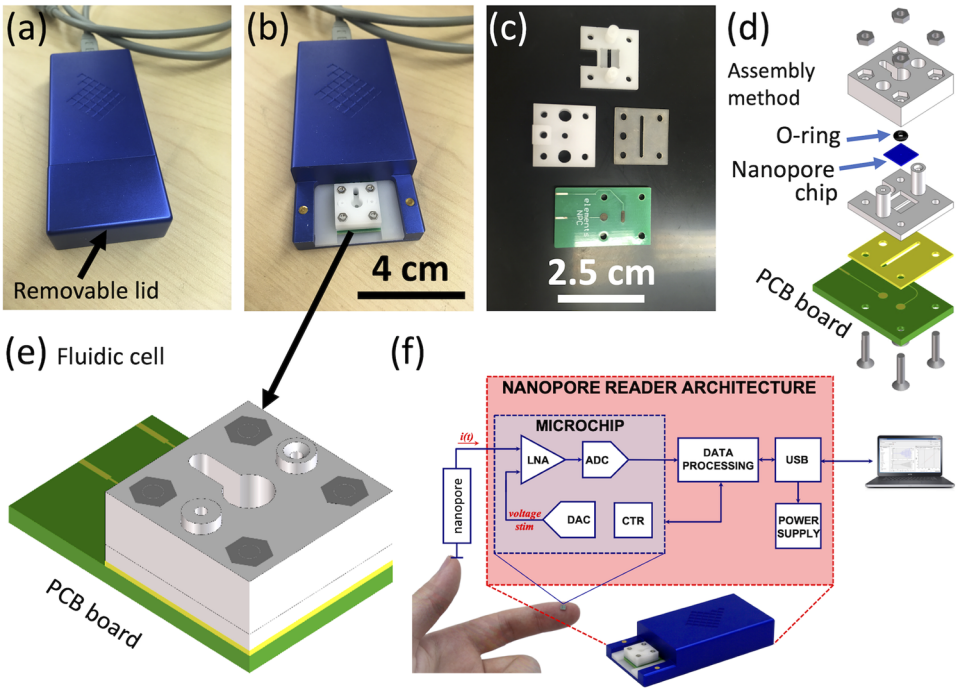

FIG. 3. (a) Photograph of the new portable mini nanopore reader and the nanopore fluidic cell we developed specifically for field use with dimension of 101 × 44 × 18 mm^3, integrating the low-noise amplifier (open input noise: 250 fA rms at 10 kHz; 2.3 pA rms at 100 kHz), digitizer, and Universal Serial Bus (USB) data link. Input current ranges are available from ±200 pA to ±200 nA, the voltage stimulus is between ±2000 mV, max sampling rate 200 k sample/s. (b) Photograph of the opened nanopore reader showing the fluidic cell (white part) inserted with a sliding connection into the reader. (c) Parts of the microfluidic cell designed to hold the 3-mm-diameter, low-noise glass chips. The white parts are made by Delrin® [PolyOxyMethylene (POM)] and the 15 × 25 mm^2 PCB board integrates the Ag/AgCl electrodes [green rectangle in (d)]. (d) and (e) Schematic 3D drawings and illustration of the assembly procedure for the parts in (b) and (c). (f) Schematic of the nanopore reader architecture discussed in the text.

Published under license by AIP Publishing

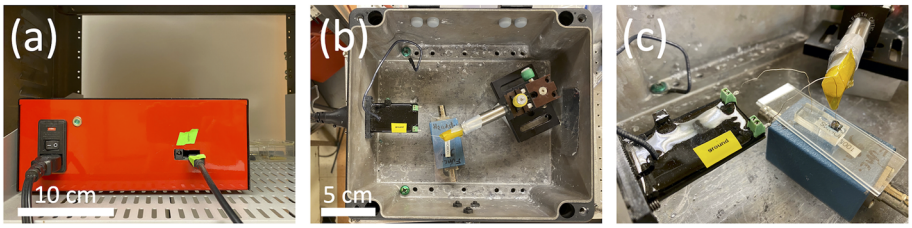

FIG. 4. Photographs of the 1 MHz bandwidth Chimera amplifier in (a) and the measurement setup in (b) and (c). Part (a) shows the stand-alone amplifier box. Parts (b) and (c) are photographs of the measurement setup inside of a thick Faraday cage housing. Inside of this housing we mounted the fluidic cell and the electrodes for ionic measurements on glass chips.

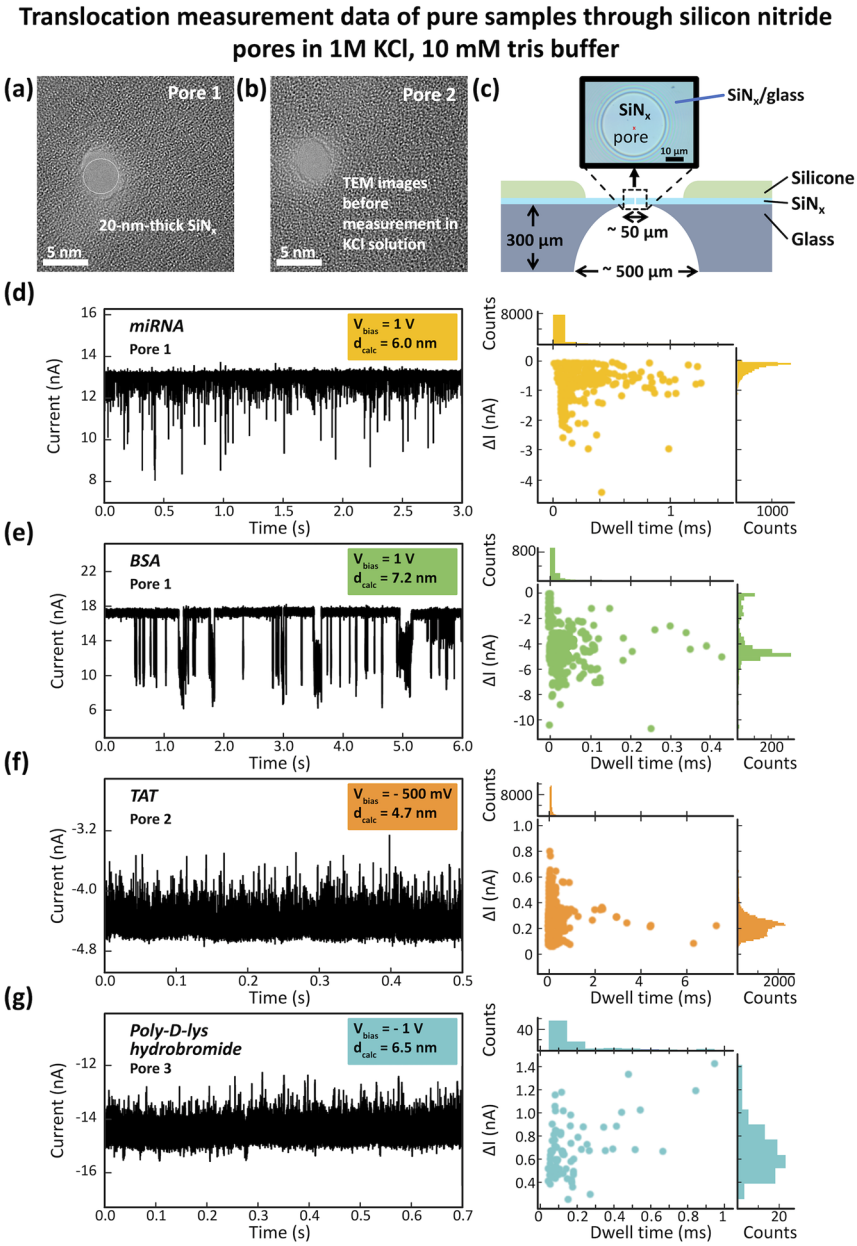

FIG. 5. Transmission electron microscope images of (a) "pore 1" used in miRNA and BSA measurements and (b) "pore 2" used in TAT measurement, and (c) the SiN_x/glass chip schematics and the optical micrograph of the circular SiN_x window in the center of the chip. Ionic current vs time traces for translocations, current and event duration histograms of (d) miRNA, (e) BSA, (f) TAT and (g) poly-D-lys-hydrobromide in 1 M KCl, 10 mM Tris buffer, pH 7.4, with voltage magnitudes and polarities applied as indicated, measured with the Chimera amplifier setup at measurement bandwidth of 1 MHz and filtered by computer to 100 kHz (4-pole Bessel filter), Fig. 4. Current vs time traces were analyzed using an open access custom-made PyPore analysis software made at the University of Pennsylvania, available at https://github.com/parkin/pypore.

Published under license by AIP Publishing

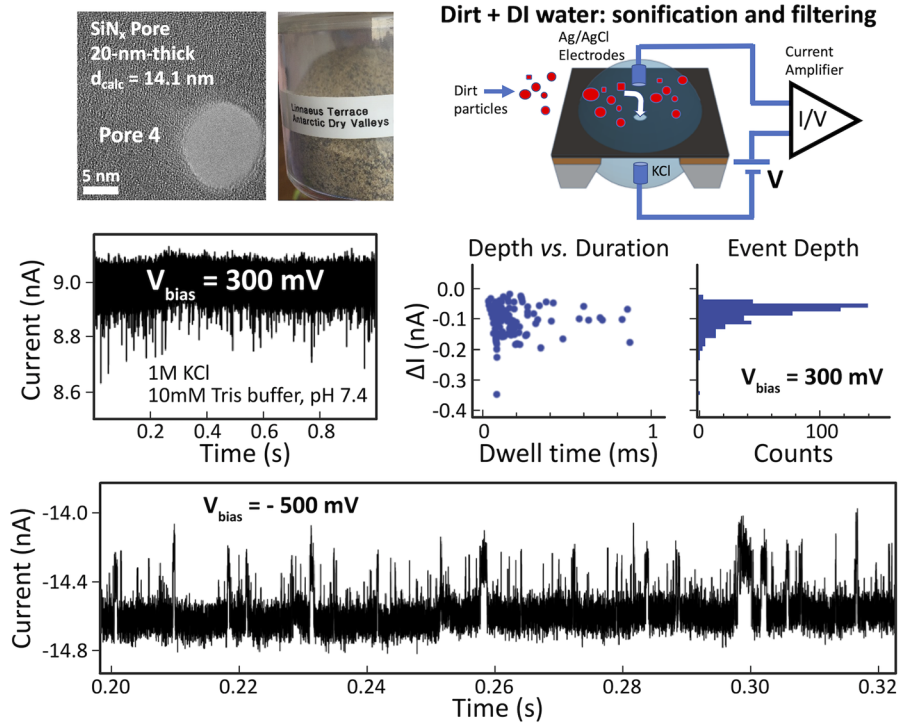

FIG. 6. Translocation measurements of Antarctic dirt particles through SiN_x nanopores measured at 1 MHz with the Chimera amplifier setup and filtered by computer to 100 kHz (4-pole Bessel filter) (Fig. 4), with other parameters indicated and discussed in the text. The TEM image of the "pore 4" used is shown and the calculated diameter is d_{calc} = 14.1 nm from the open pore current (assuming nanopore thickness t = 20 nm). Current vs time traces are shown for V = +300 mV and V = −500 mV, and the histogram of current amplitudes and scatter plot of current amplitudes vs dwell times (event durations) are shown for the current trace taken at V = +300 mV.

using suction. The chip is then loaded into the fluidic cell and wet immediately in the salt solution.

The linear current-voltage characteristics of individual pores are measured at applied voltages up to 1 V and open pore conductance is calculated. The open pore conductance, G, is well described[61] by

$$G = \frac{1}{\nu} = \sigma\left[\frac{4t}{\pi d^2} + \frac{1}{d}\right]^{-1}, \quad (1)$$

where I is the measured ionic current and V is the applied voltage. Other parameters include the ionic solution conductivity ($\sigma \sim 11.8$ S/m for 1 M KCl at room temperature), nanopore diameter, d, and

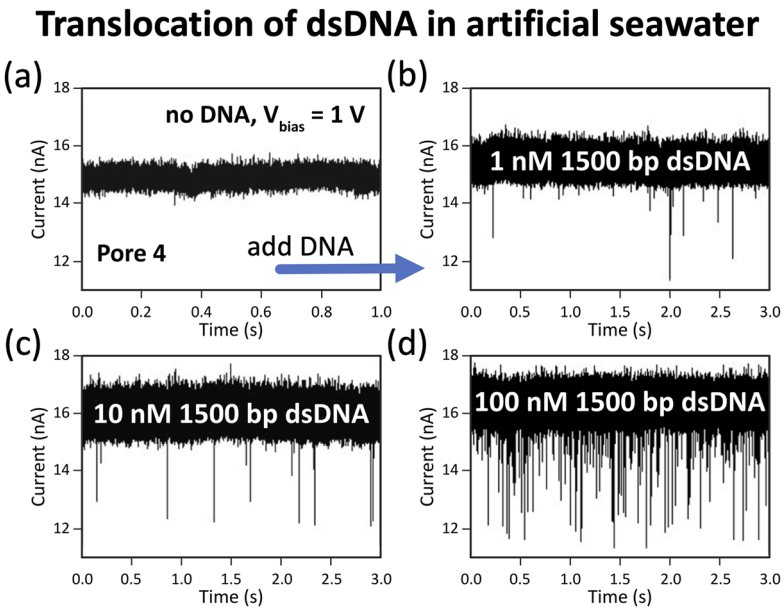

FIG. 7. Current vs time traces showing double-stranded DNA measurements in artificial seawater (a) without any added analytes, (b) with 1 nM 1500 bp dsDNA, (c) with 10 nM 1500 bp dsDNA, (d) with 100 nM 1500 bp dsDNA at +1 V transmembrane bias voltage, measured at 1 MHz with the Chimera amplifier setup and filtered by computer to 100 kHz (4-pole Bessel filter) (Fig. 4). *Cis* side of solution was RICCA® Synthetic Seawater, ASTM D 1141 (artificial seawater). *Trans* side was 1M NaCl. The pore used was "pore 4," which was also used in the Antarctic dirt measurement (Fig. 6). The RICCA Synthetic Seawater ASTM D 1141 we use here is made from water, sodium chloride, magnesium chloride hexahydrate, sodium sulfate, calcium chloride dihydrate, potassium chloride, sodium bicarbonate, potassium bromide, strontium chloride hexahydrate, boric acid, sodium hydroxide, and sodium fluoride.

Published under license by AIP Publishing

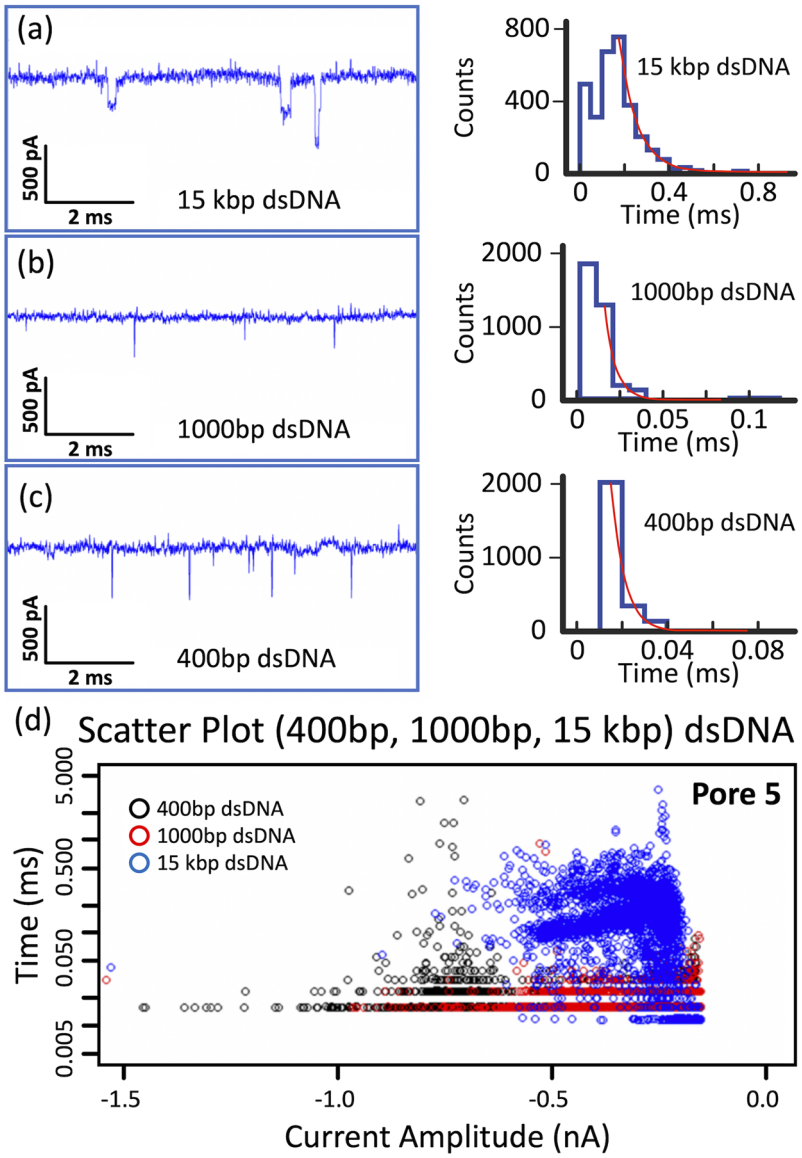

FIG. 8. dsDNA fragment translocation data obtained with a 17-nm-diameter SiN_x pore at V = +200 mV, 1M KCl (10 mM Tris buffer, 1 mM EDTA and pH 8.0) for (a) 15 kbp, (b) 1000 bp, and (c) 400 bp dsDNA, and corresponding event duration histograms measured at 100 kHz bandwidth with the portable nanopore reader (Fig. 3). Red curves in (a)–(c) are exponential fits to obtain the characteristic dwell times 94 ± 7 μs, 29 ± 9 μs, and 9 ± 6 μs for data in (a)–(c). (d) Corresponding scatterplots of dsDNA event durations vs event depth for 400, 1000, and 15 000 bp dsDNA fragments.

nanopore thickness, t (t = 20 nm). From Eq. (1) and by assuming that the pore thickness is equal to the membrane thickness, we can estimate the pore diameter, d_{calc}, as in

$$d_{calc} = \frac{G}{2\sigma}\left(1 + \sqrt{1 + \frac{16\sigma t}{G\pi}}\right) \quad (2)$$

and compare this calculated value from the ionic measurement with the experimental diameter, d_{TEM}, from TEM imaging prior to ionic measurements.

C. Nanopore setups: New portable nanopore reader (100 kHz bandwidth) and Chimera amplifier (1 MHz bandwidth) setups

Figure 3 describes the new nanopore reader prototype [Fig. 3(a)] and the nanopore fluidic cell [Fig. 3(e)], which we designed and built here as a compact and hand-held instrument for high sensitivity nanopore measurements for environmental samples. The core technology is based on a custom CMOS microchip (Elements srl), which integrates in 10 mm^2 a low-noise current amplifier [LNA in Fig. 3(f)] for signal amplification and conversion from current to voltage, an Analog to Digital Converter [ADC in Fig. 3(f)] for signal data sampling and a Digital to Analog Converter [DAC in Fig. 3(f)] for voltage stimulus generation. The microchip is fully controlled by an SPI digital data serial interface, which allows us to set the current acquisition ranges, the sampling rate, the voltage stimulus to be applied to the nanopore, and the voltage offset correction to compensate the Ag/AgCl voltage offset at the electrodes of the fluidic cell. The nanopore reader integrates, inside a single PCB board, the previously described custom CMOS microchip, a spring-load connector to connect the fluidic cell when this is slid into the reader, a data processing unit, and a USB controller for

Published under license by AIP Publishing

data link to a personal computer. The PCB board reader is encased by aluminum housing for noise shielding [blue cover in Fig. 3(a)], no additional Faraday cage is required even for low currents level of detection (below 1 pA, depending on the sampling rate). A sliding system allows easy mounting and connection of the fluidic cell to the reader, minimizing the parasitic capacitances that contribute to the current noise in ionic current measurements. The aluminum removable lid [Fig. 3(a)] provides the shielding to the nanopore sensor. The final dimensions of the reader make it a portable device, useful for on-field analysis. The nanopore fluidic cell [Fig. 3(d)] is composed of the two white parts made by Delrin [PolyOxyMethylene (POM)], each one has channels and wells to host the electrolyte. The white bottom part in Fig. 3(d) presents a rectangle housing where the nanopore chip sits and is sealed by an O-ring to the top white part. The two white parts are assembled together with the nanopore chip in between, and this part is finally assembled with the 15 × 25 mm^2 PCB board with integrated Ag/AgCl electrodes [green rectangle in Fig. 3(d)] using a laser-cut silicon gasket [yellow square in Fig. 3(d)] and four screws and bolts. Compared with typical nanopore measurement setups (such as Axon, Sutter, or HEKA amplifiers), where usually the amplifier and digitizer are 19 in.-rack instruments designed only for laboratory setups and not for portable or on-field applications, this new instrument is suitable for the next generation of point-of-care devices facilitated by the microchip-based technology, allowing a similar measurement performances in terms of signal-to-noise levels and high sensitivity for single-molecule detection to the standard laboratory equipment such as Axon amplifiers. Compared with other hand-held USB instruments like Oxford Nanopore's MinION,[67] the nanopore reader offers only one input channel but with higher sampling rate (200 k sample/s), more flexibility in selecting the input gain (variable between four current ranges available from ±200 pA to ±200 nA), and a fully controllable voltage stimulus between ±2000 mV, for a range of different application needs. The two instruments are designed for different applications: MinION was optimized and dedicated to DNA sequencing and the nanopore reader is a more general instrument for nanoparticle and single molecule detection. For this reason, a detailed comparison between the two instruments is not acutely relevant because of their different fields of potential applications. Briefly, the MinION uses a fluidic cell with about a thousand identical biological nanopores, while the nanopore reader allows an easy replacement of different kinds of nanopores, from biological to solid state, thanks to the fluidic cell design where the nanopore chip can be easily and rapidly exchanged. Another important aspect is that the nanopore reader's fluidic cell allows the access to both the fluidic compartments separated by the nanopore chip, while the MinION fluidic cell allows the fluidic access only to the top-fluidic side of the nanopore array while the bottom-fluidic side is filled with the unchangeable electrolyte from the factory.

Figures 4(a)–4(c) show photographs of the higher-bandwidth Chimera amplifier setup including the stand-alone amplifier [Fig. 4(a)] and the Faraday cage with the fluidic cell and electrodes [Figs. 4(b) and 4(c)] for ionic current measurements up to bandwidth of 1 MHz, developed in 2013 as a stand-alone module and first used with solid-state nanopores to differentiate short single-stranded DNA homopolymers.[28] The use of the Chimera amplifier in this work was motivated by its higher bandwidth compared with the portable device, 1 MHz vs the portable reader's bandwidth of 200 kHz, to push the limits of detection, particularly for measurements of the environmental samples (Antarctic dirt). The 1 MHz bandwidth is not reachable with older amplifier models (such as Axon 200 or HEKA).

For data collection at 1 MHz and higher bandwidths,[32,61] the noise is dominated by the overall capacitance. At sufficiently high bandwidths, the root-mean-square current noise of the baseline ionic current[61] is $\propto B^{3/2}$ C v_n, where B is the bandwidth of measurement, v_n is the input-referred voltage noise of the amplifier, and C is the total capacitance at the input of the amplifier and typically consists of the chip capacitance, C_{chip}, the wiring capacitance, C_w, and the capacitance of the amplifier, C_{amp}. Improvements in signal-to-noise ratio are therefore obtained by decreasing this baseline noise via new chip and amplifier designs and by increasing the signal via fabrication of thinner pores. Nanopore chip capacitance is made to be comparable or smaller than the amplifier capacitance[30] by increasing the thickness of insulating layers on the chip[26,30,32] and ultimately by replacing the typical silicon chips by glass chips[31,61] as presented here (Fig. 1).

III. RESULTS AND DISCUSSION

In Table I, we list the calculated diameters, d_{calc}, and TEM-measured diameters, d_{TEM}, of all nanopores for the following Figs. 5–8.

In this work, we use and list both the TEM-measured diameters and the calculated diameters from ionic measurements (assuming thickness t = 20 nm). Both serve as good but not perfect estimates of the nanopore diameter, and both have their corresponding sources of errors. The TEM-measured diameter corresponds to the pore in vacuum, right after drilling; the pore can be contaminated once it is taken out of vacuum or it can change over time in ionic solutions. The calculated diameter, on the other hand, represents a more relevant estimate at the time of the ionic measurements, but its value from Eq. (2) depends on the assumed value of the pore thickness (t) that may be different than the membrane thickness, in this case 20 nm.

The pore diameter, d_{calc}, was estimated using Eq. (2) from the main text. When different solutions were used in *trans* and *cis* sides, we took the average ionic solution conductivity of both sides. For

TABLE I. List of calculated diameters, d_{calc}, and TEM diameters, d_{TEM}, of nanopores.

Pore no.	Figure no.	d_{calc} (nm)	d_{TEM} (nm)
PORE 1	Figure 5(d)	6.0	3.8 ± 0.1
	Figure 5(e)	7.2	3.8 ± 0.1
PORE 2	Figure 5(f)	4.7	3.7 ± 0.1
PORE 3	Figure 5(g)	6.5	1.7 ± 0.1
PORE 4	Figure 6	14.1	10.6 ± 0.1
	Figure 7(a)	9.3	10.6 ± 0.1
	Figure 7(b)	9.3	10.6 ± 0.1
	Figure 7(c)	9.3	10.6 ± 0.1
	Figure 7(d)	9.3	10.6 ± 0.1
PORE 5	Figure 8	17.0	2.6 ± 0.1

Published under license by AIP Publishing

example, in Fig. 7, the *cis* side of solution was artificial seawater (σ ~ 6 S/m), while the *trans* side was 1M NaCl (σ ~ 8.5 S/m). So, we used an average conductivity value of ~7.2 S/m to estimate the pore diameter, d_{calc}. Some nanopores have enlarged during the piranha cleaning and/or subsequent cleaning and measurement steps. Their calculated diameter, d_{calc}, is similar or larger than d_{TEM} (Table I); d_{TEM} was measured in vacuum right after TEM drilling. Pores 3 and 5 significantly expanded by the time we performed ionic measurements in Figs. 5(g) and 8, about one month after the pores were drilled in the TEM. Pores 3 and 5 were also additionally cleaned with oxygen plasma for 30 s at 30–50 W RF power and then stored in isopropyol alochol (IPA), followed by two sets of DNA translocation measurements, which all likely resulted in larger diameter pores by the time the data sets in Figs. 5 and 8 were taken, hence likely explaining the apparent discrepancy between d_{calc} and d_{TEM} for these pores.

A. Translocation measurement data on pure samples (clean analytes) through silicon nitride pores

In Fig. 5, we show translocation data of four pure analytes measured with a Chimera amplifier setup (Fig. 4). In this experiment, we used two positively charged analytes (poly-D-lys-hydrobromide and TAT) and two negatively charged analytes (miRNA and BSA). We started this experiment by making 18 SiN_x chips with pore diameters from 1.6 nm to 11 nm, as determined from TEM images. The pores were TEM drilled in 20-nm-thick SiN_x circular membranes on glass chips. Of the 18 chips, 13 chips gave a stable pore current, corresponding to a yield of 72% of working pores. This number can be used for further experiments as estimated yield. For example, to measure reliable data from 1000 working pores, we would need to perform experiments on ~1400 pores. Beyond speculative interpretations, we do not have direct and conclusive measurements on what causes a particular pore to have unstable currents. For example, Smeets *et al.* in 2007[40] speculated early on that the 1/f current-noise in silicon nitride pores originates from hydrophobic regions within the pore interior.

Figure 5 shows ionic current vs time traces for translocations of miRNA, BSA, TAT, and poly-D-lys-hydrobromide in 1M KCl, 10 mM Tris buffer, pH 7.4, with voltage magnitudes and polarities applied as indicated at measurement bandwidth of 1 MHz and digitally filtered by computer to 100 kHz (4-pole Bessel filter). With no analytes, we measure a flat control signal. As expected, when we turn on the voltage, the negative analytes were detected only for a positive applied voltage (miRNA and BSA) and the positive analytes were detected only for a negative applied voltage (poly-D-lys-hydrobromide and TAT). Pore diameters were initially measured from the TEM images. The TEM images of "pore 1" and "pore 2" are shown for illustration—the white circle shows an approximate circular fit to the pore 1 image, from which we measure the initial diameter. We also estimate the diameter from the open pore conductance, d_{calc}, and this number is given for each trace in Fig. 5. The calculated diameter, d_{calc}, is similar or larger than the TEM diameter, d_{TEM} (Table I), which was measured in vacuum before ionic measurements. This can indicate that some pores may be enlarging during the cleaning and/or measurement steps; $d_{calc} > d_{TEM}$ may also mean that the pore thickness is smaller than the membrane thickness, which can be attributed to its hourglass shape. A more accurate estimate of the thickness of TEM-drilled pores was shown to be ~1/3 of the membrane thickness—this was established using translocations of DNA molecules of known size to calibrate the nanopore size.[42] In our case, one-third of the membrane thickness is ~7 nm.

In our measurements, the open pore current is used to recalibrate the pore diameter assuming a constant thickness. For example, "pore 1" was used for both miRNA and BSA measurements. First, we measured miRNA, then rinsed the pore, and measured BSA. The calculated diameter increased from d_{calc} = 6–7.2 nm over the course of these experiments (assuming that the pore thickness is equal to the membrane thickness t = 20 nm). We further estimate the size of these analytes, D, based on the current blockade percentage relative to the open pore current, $\Delta I/I_{open\ pore} \sim D^2/d_{calc}{}^2$. The estimated diameters of each analyte are shown, respectively: miRNA, 0.7 nm; BSA, 3.9 nm; TAT, 1.0 nm; and poly-D-lys-hydrobromide, 1.2 nm. The diameter of BSA matches the previously reported diameter of 40 Å.[68]

Data in Fig. 5 show how different pore diameters can be used for particular analytes even with the same pores. To maximize the signal-to-noise ratio, the pore diameter should be as small as possible but large enough to allow translocations without too much pore clogging by the analyte. Additionally, the voltage sign that allows translocations reveals the charge of the molecule passing through (there are no detected translocations for the opposite polarity, as expected). The open pore current (no analyte present) matches the value from the simple calculation [Eq. (1)] and the average magnitude of the blocked current can be used to estimate the size of the analyte as it passes through the pore. These data also illustrate two clear advantages of silicon nitride nanopores over biological pores for the detection of nanometer-sized particles. First, we can easily make pores that are bigger than protein pores that are typically ~1–2 nm in diameter. Second, the silicon nitride pore diameter can be in principle adjusted in a large range over five orders of magnitude in size, from sub-nanometer to micrometers, for the detection of analytes in a wide range of sizes, from ions and molecules to larger viruses.

B. Translocation measurement data of environmental sample (Antarctic dirt) through silicon nitride pores

Figure 6 shows translocation data obtained from the Antarctic dirt sample, provided by NASA Ames. Similar testing and evaluation of signal-to-noise ratio can be utilized for other environmental samples, including more advanced data analysis approaches. The sample was prepared in the following way: 0.13 g/ml of Linnaeus Terrace Antarctic dirt sample (Antarctic Dry Valleys) was placed into 50 ml of DI water and ultra-sonicated vigorously. The resulting solution was filtered through a syringe [Whatman syringe filter, Anotop TM5 0.1 μm, General Electric Life Science (www.gelifesciences.com)] that filters out particles greater than 100 nm. The listed specifications for this filter include that Anotop is a hydrophilic membrane with excellent organic solvent compatibility, suitable for use with both aqueous and organic samples, and that the membrane has a tight pore-size distribution. However, no specific numbers are given how sharp is the cutoff for the distribution of the pore sizes in the membrane, so it is possible that this filter also rejects some particles smaller than 100 nm. Opposite side solution was 1M KCl, 10 mM Tris buffer, pH 7.4. Figure 6 shows the TEM image of the nanopore used ("pore 4"),

Published under license by AIP Publishing

whose diameter was 14.1 nm, calculated from the open pore current and equation for conductance, *G*, given by Eq. (1). The photograph of the dirt sample prior to solution preparation and the schematic of the measurement are also shown.

We have applied both voltage polarities to see if we can detect any negatively or positively charged particles from the sample. Here, we show two examples of ionic current vs time traces for V = +300 mV applied to the bottom electrode, corresponding to translocations of negative particles, as well as another trace for the opposite polarity, at V = −500 mV, corresponding to translocations of positive particles. Without the dirt introduced, the open pore current signal is just flat and the I_{rms} noise is about 0.1 nA at measurement bandwidth of 1 MHz and filtered by computer to 100 kHz (4-pole Bessel filter). When the dirt solution is introduced and voltage is applied, we observe translocations spikes occurring.

From nanopore measurements alone, we cannot determine what molecules these translocation events correspond to, as the nanopores are only giving us approximate information about the size and sign of the charge of the molecules we are detecting. Such nanopore sensors are envisioned to be used in combination with other instruments to triangulate and narrow down their properties and origin. However, it is interesting to speculate about the properties of the entities measured from the data. Even though the pore was small, ~14.1 nm in diameter, and we filtered the sample only with a 100-nm filter, the pore did not clog quickly and we were able to observe many translocation events for both voltage polarities. From the data set at V = −500 V, it does look like there are some longer duration events that could correspond to molecules clogging and sticking to the pore.

In the data set at V = +300 mV, the open pore current is ~9 nA, corresponding to conductance of ~30 nS. We see translocation spikes that correspond to a current drop ~0.2–0.3 nA, corresponding to ~2%–3% of the open pore signal. From this percentage, we can estimate that the average diameter, D, of translocating negative particles estimated by $D^2/(14.1)^2$ ~ 2%–3%, from which we get D (cross sectional size of the translocating negative particles) ~1.1–1.3 nm. For the case of opposite polarity at V = −500 mV, a similar estimate gives us a size of translocating positive particles $D^2/(14.1)^2$ ~ (0.2–0.4 nA)/14.6 nA − 1.4%–2.7% and we estimate the diameter of the positive particles to be D ~ 1.7–2.3 nm. The fact that we do not see more clogging, or deeper translocation events, means that translocating molecules had a size in the pore of ~2 nm. Otherwise, a pore of ~14 nm diameter would clog completely and quickly. These results are encouraging for future studies as they show steady translocations with a large number of translocation events from dirt samples, relevant for field use.

C. Translocation measurement data using synthetic seawater with and without DNA molecules through silicon nitride pores

We show ionic current vs time data obtained from "pore 4." This is the same pore used in the Antarctic dirt tests (Fig. 6). It is important to note that these pores can be *rinsed* and *reused*, thus increasing their lifetime and usefulness. In these experiments, pores were rinsed thoroughly in DI water and then isopropanol, and they were stored in isopropanol. We used synthetic seawater (RICCA, synthetic seawater ASTM D 1141, pH at 25 °C: 8.20–8.25), a laboratory sample that mimics seawater, to determine if the solution alone would act as an electrolyte for nanopore sensing. The salt constituents of the RICCA Synthetic Seawater (www.syntheticseawater.com) used here are listed in the caption of Fig. 7. We measured the conductivity of synthetic seawater to be 5 S/m and at room temperature with the Accumet XL-20 pH conductivity meter, which is equivalent to 40.09‰ of salinity,[53] similar to the reported value of 35.00‰ in previous measurement carried by Kester *et al.*[54] Artificial seawater recipes have been improved in the 1960s to closely mimic the natural seawater composition and to provide a reproducible and stable solution of known composition and pH.[54]

The open pore conductance of the pore was ~15 nS in artificial seawater in Fig. 7(a), compared with 29.2 nS in 1 M KCl in Fig. 6, in good agreement with the measured conductivity, 6 S/m vs 11.8 S/m, respectively. We check that the pore was cleaned well from the previous analyte by measuring its open pore current again and seeing that there are no translocation signals from any contamination and that the background current noise level is the same as for the freshly made pore. We then proceed to put the next analyte.

The four panels in Fig. 7 show current vs time at applied voltage of V = +1 V for synthetic seawater [Fig. 7(a)] and spiked with 1 nM, 10 nM, and 100 nM of 1500 bp double-stranded DNA (ThermoScientific®) [Figs. 7(b)–7(d)]. The choice of DNA here as the analyte is motivated by ideas that life may require long charged polymers[45] to evolve. DNA is the information storage molecule here on Earth, and therefore, DNA seems like a good test case for other informational polymers. With no DNA, the current vs time trace is flat with no noticeable spikes. As the DNA is added, we immediately observe clear translocation events that increase in frequency as the DNA concentration is increased from Figs. 7(b)–7(d), in steps of one order of magnitude in concentration. The rates for dsDNA translocation events measured in the artificial seawater were 0.6 events/s, 2.6 events/s, and 22 events/s for 1 nM, 10 nM, and 100 nM concentrations, respectively. Extracting the translocation rate from these samples and assuming linear scaling of translocation with concentration of DNA,[7] we come to a limiting rate of 1 translocation/10 min at a concentration of ~10 pM dsDNA. It is important to note that this rate is dependent on several factors that could readily be modified to change the capture rate. Factors that can influence capture rate include the applied voltage and electrostatic focusing using asymmetric salt gradients.[7]

We can perform further analysis of these data. For example, we see shallower and deeper events. We also know that the pore is wide enough to allow dsDNA folding. For example, the maximum percentage blocked is ~30%. In Fig. 7(d), for example, the current blocked is ~4.5 nA (signal conductance is 4.5 nS since the voltage is 1 V), and the open pore current is ~16.5 nA. For a cross sectional dimension D of the analyte, we can estimate from $D^2/(9.3)^2$–30%, D ~ 5 nm. This likely corresponds to folded dsDNA (dsDNA is about 2.2 nm in diameter) for the deeper events and single-file translocations for the shallower events. Further measurements will be pursued in the future with synthetic seawater to and address limits of sensitivity and specificity of detection, which may require further improvements of the experimental setup and nanopore chips. Additional work should be focused on modeling data from synthetic

Published under license by AIP Publishing

seawater for various analytes. Data in Fig. 7 confirm the use of synthetic seawater as a good electrolyte for nanopore measurements and to detect DNA. The artificial synthetic seawater itself does not introduce more noise compared with pure salt solution such as 1 M KCl, typically used in a laboratory setting.

While the best stand-alone amplifier setups are currently superior due to their high bandwidth and low-noise operation such as the Chimera amplifier used here or the recently developed CNP2 amplifier operating at 10 MHz,[32,61] for environmental and field use, it is also important to have a hand-held, light, and practical setup. For that purpose, we also developed the nanopore reader that operates up to 100 kHz bandwidth, which is sufficient to detect analytes presented in this work and should facilitate further uses of solid-state pores for environmental testing.

Figure 8 shows examples of data collected on dsDNA fragment translocations obtained with a 17-nm-diameter SiN_x pore at applied voltage V = +200 mV using 1M KCl (10 mM Tris buffer, 1 mM EDTA and pH 8.0) for 15 kbp [Fig. 8(a)], 1000 bp [Fig. 8(b)], and 400 bp [Fig. 8(c)] dsDNA, and corresponding event duration histograms measured at 200 kHz sampling rate, with an equivalent bandwidth of 100 kHz. The nanopore chip was flushed with IPA and DI water between introduction of new analytes to ensure that the nanopore is clean before the next measurement. DNA concentration for the data in Fig. 8 was 200 nM for all three DNA types.

Event duration histograms are fitted by exponential decay functions to obtain the characteristic dwell times of 94 ± 7 μs, 29 ± 9 μs, and 9 ± 6 μs [red fit lines in Figs. 8(a)–8(c)], showing that the 15 000 bp dsDNA produces the longest translocation events. Corresponding scatterplots of dsDNA event durations vs event current amplitudes (or event depths) for these dsDNA fragments are shown in Fig. 8(d). The three datasets can be distinguished with the average event amplitudes and average events durations increasing from 400 bp [black points in Fig. 8(d)] to 15 000 bp data [blue points in Fig. 8(d)].

IV. CONCLUSIONS

In summary, here, we demonstrated the use of silicon nitride pores with yield (pores that gave stable currents) ~70% in 20-nm-thick silicon nitride membranes on fused-silica chips to translocate positively and negatively charged pure laboratory samples containing a single analyte, including DNA in artificial seawater toward mimicking natural seawater conditions. We also used these pores to detect ~1-nm-size particulates present in the pre-filtered Antarctic dirt that was mixed with distilled water and prefiltered. The 20-nm-membrane thickness allows the pores to be robust enough, yet still highly sensitive to nanometer-scale molecules. We have combined low-noise glass nanopore chips with a new nanopore reader that we have designed and built on a centimeter scale that is portable, easy to use, and facilitates low-noise measurements up to 100 kHz bandwidth. The combined chips and the nanopore reader are ideally suited for field applications where size, portability, and robustness are important factors. Future applications include the detection and analysis of other pre-filtered environmental samples such as in ocean water or soil and for general field use. In addition, given the previous successful flight heritage of silicon nitride as a suitable material for space applications, these pores are particularly interesting candidates for the detection of extraterrestrial life in outer space, in concert with many other instruments that can be used to narrow down the properties and origin of molecules being detected. The use of these nanopore chips presented can be in the future extended to a broad range of environmental samples and pores can be cleaned, reused, and also stored for a long time.

AUTHOR'S CONTRIBUTIONS

The manuscript was written through contributions of all authors. All authors have given approval to the final version of the manuscript.

ACKNOWLEDGMENTS

The glass chips and nanopores were fabricated at the Pennovation Center and at the University of Pennsylvania's Singh Center for Nanotechnology and at Rutgers University by Goeppert LLC. We thank Dr. Chris McKay from NASA Ames for providing samples of the Linnaeus Terrace dirt from Antarctic Dry Valleys. We also thank Jacob Swett at the University of Oxford for useful discussions and Michele Rossi, previously at Elements, SRL, for help with the portable nanopore reader. The nanopore reader and fluidic cell were developed here in collaboration with Elements, SRL, Italy. The work was supported by NASA SBIR Phase I No. S.11-3492 (2018-1) "Detecting life in ocean worlds with low-capacitance solid-state nanopores." This work was carried out in part at the Singh Center for Nanotechnology, which is supported by the NSF National Nanotechnology Coordinated Infrastructure Program under Grant No. NNCI-1542153.

REFERENCES

[1] J. J. Kasianowicz, E. Brandin, D. Branton, and D. W. Deamer, Proc. Natl. Acad. Sci. U. S. A. **93**, 13770 (1996).
[2] D. Branton, D. W. Deamer, A. Marziali, H. Bayley, S. A. Benner, T. Butler, M. Di Ventra, S. Garaj, A. Hibbs, X. Huang, S. B. Jovanovich, P. S. Krstic, S. Lindsay, X. S. Ling, C. H. Mastrangelo, A. Meller, J. S. Oliver, Y. V. Pershin, J. M. Ramsey, R. Riehn, G. V. Soni, V. Tabard-Cossa, M. Wanunu, M. Wiggin, and J. A. Schloss, Nat. Biotechnol. **26**, 1146 (2008).
[3] M. Akeson, D. Branton, J. J. Kasianowicz, E. Brandin, and D. W. Deamer, Biophys. J. **77**, 3227 (1999).
[4] O. K. Dudko, J. Mathé, A. Szabo, A. Meller, and G. Hummer, Biophys. J. **92**, 4188 (2007).
[5] K. Healy, B. Schiedt, I. P. Morrison, and A. P. Morrison, Nanomedicine **2**, 875 (2007).
[6] T. Z. Butler, M. Pavlenok, I. M. Derrington, M. Niederweis, and J. H. Gundlach, Proc. Natl. Acad. Sci. U. S. A. **105**, 20647 (2008).
[7] M. Wanunu, W. Morrison, Y. Rabin, A. Y. Grosberg, and A. Meller, Nat. Nanotechnol. **5**, 160 (2010).
[8] R. Kawano, A. E. P. P. Schibel, C. Cauley, and H. S. White, Langmuir **25**, 1233 (2009).
[9] L.-Q. Gu and J. W. Shim, Analyst **135**, 441 (2010).
[10] Z. S. Siwy and S. Howorka, Chem. Soc. Rev. **39**, 1115 (2010).
[11] S. W. Kowalczyk, A. R. Hall, and C. Dekker, Nano Lett. **10**, 324 (2010).
[12] K. R. Lieberman, G. M. Cherf, M. J. Doody, F. Olasagasti, Y. Kolodji, and M. Akeson, J. Am. Chem. Soc. **132**, 17961 (2010).
[13] C. A. Merchant, K. Healy, M. Wanunu, V. Ray, N. Peterman, J. Bartel, M. D. Fischbein, K. Venta, Z. Luo, A. T. C. C. Johnson, and M. Drndić, Nano Lett. **10**, 2915 (2010).
[14] D. W. Deamer and M. Akeson, Trends Biotechnol. **18**, 147 (2000).
[15] S. Garaj, W. Hubbard, A. Reina, J. Kong, D. Branton, and J. A. Golovchenko, Nature **467**, 190 (2010).

Published under license by AIP Publishing

[16]U. Mirsaidov, J. Comer, V. Dimitrov, A. Aksimentiev, and G. Timp, Nanotechnology **21**, 395501 (2010).
[17]J. E. Reiner, J. J. Kasianowicz, B. J. Nablo, and J. W. F. F. Robertson, Proc. Natl. Acad. Sci. U. S. A. **107**, 12080 (2010).
[18]M. Wanunu, Phys. Life Rev. **9**, 125 (2012).
[19]W. Timp, J. Comer, and A. Aksimentiev, Biophys. J. **102**, L37 (2012).
[20]E. A. Manrao, I. M. Derrington, A. H. Laszlo, K. W. Langford, M. K. Hopper, N. Gillgren, M. Pavlenok, M. Niederweis, and J. H. Gundlach, Nat. Biotechnol. **30**, 349 (2012).
[21]S. W. Kowalczyk, D. B. Wells, A. Aksimentiev, C. Dekker, P. Susan, S. W. Kowalczyk, D. B. Wells, A. Aksimentiev, and C. Dekker, Nano Lett. **12**, 1038 (2012).
[22]R. Wei, T. G. Martin, U. Rant, and H. Dietz, Angew. Chem., Int. Ed. **51**, 4864 (2012).
[23]M. Langecker, V. Arnaut, T. G. Martin, J. List, S. Renner, M. Mayer, H. Dietz, and F. C. Simmel, Science **338**, 932 (2012).
[24]B. Luan, D. Wang, R. Zhou, S. Harrer, H. Peng, and G. Stolovitzky, Nanotechnology **23**, 455102 (2012).
[25]A. Meller and D. Branton, Electrophoresis **23**, 2583 (2002).
[26]J. K. Rosenstein, M. Wanunu, C. A. Merchant, M. Drndic, and K. L. Shepard, Nat. Methods **9**, 487 (2012).
[27]G. M. Cherf, K. R. Lieberman, H. Rashid, C. E. Lam, K. Karplus, and M. Akeson, Nat. Biotechnol. **30**, 344 (2012).
[28]K. Venta, G. Shemer, M. Puster, J. A. Rodríguez-Manzo, A. Balan, J. K. Rosenstein, K. Shepard, and M. Drndić, ACS Nano **7**, 4629 (2013).
[29]Y. He, M. Tsutsui, R. H. Scheicher, F. Bai, M. Taniguchi, and T. Kawai, ACS Nano **7**, 538 (2013).
[30]A. Balan, B. Machielse, D. Niedzwiecki, J. Lin, P. Ong, R. Engelke, K. L. Shepard, and M. Drndić, Nano Lett. **14**, 7215 (2014).
[31]A. Balan, C.-C. Chien, R. Engelke, and M. Drndić, Sci. Rep. **5**, 17775 (2015).
[32]S. Shekar, D. J. Niedzwiecki, C.-C. Chien, P. Ong, D. A. Fleischer, J. Lin, J. K. Rosenstein, M. Drndić, and K. L. Shepard, Nano Lett. **16**, 4483 (2016).
[33]M. Jain, S. Koren, K. H. Miga, J. Quick, A. C. Rand, T. A. Sasani, J. R. Tyson, A. D. Beggs, A. T. Dilthey, I. T. Fiddes, S. Malla, H. Marriott, T. Nieto, J. O'Grady, H. E. Olsen, B. S. Pedersen, A. Rhie, H. Richardson, A. R. Quinlan, T. P. Snutch, L. Tee, B. Paten, A. M. Phillippy, J. T. Simpson, N. J. Loman, and M. Loose, Nat. Biotechnol. **36**, 338 (2018).
[34]G. Danda and M. Drndić, Curr. Opin. Biotechnol. **55**, 124 (2019).
[35]A. J. Storm, J. H. Chen, X. S. Ling, H. W. Zandbergen, and C. Dekker, Nat. Mater. **2**, 537 (2003).
[36]D. Fologea, M. Gershow, B. Ledden, D. S. McNabb, J. A. Golovchenko, and J. Li, Nano Lett. **5**, 1905 (2005).
[37]U. F. Keyser, B. N. Koeleman, S. Van Dorp, D. Krapf, R. M. M. M. Smeets, S. G. Lemay, N. H. Dekker, and C. Dekker, Nat. Phys. **2**, 473 (2006).
[38]M. Rhee and M. A. Burns, Trends Biotechnol. **24**, 580 (2006).
[39]J. W. F. Robertson, C. G. Rodrigues, V. M. Stanford, K. A. Rubinson, O. V. Krasilnikov, and J. J. Kasianowicz, Proc. Natl. Acad. Sci. U. S. A. **104**, 8207 (2007).
[40]R. M. M. Smeets, U. F. Keyser, N. H. Dekker, and C. Dekker, Proc. Natl. Acad. Sci. U. S. A. **105**, 417 (2008).
[41]K. M. Halverson, R. G. Panchal, T. L. Nguyen, R. Gussio, S. F. Little, M. Misakian, S. Bavari, and J. J. Kasianowicz, J. Biol. Chem. **280**, 34056 (2005).
[42]M. Wanunu, T. Dadosh, V. Ray, J. Jin, L. McReynolds, and M. Drndić, Nat. Nanotechnol. **5**, 807 (2010).
[43]K. E. Venta, M. B. Zanjani, X. Ye, G. Danda, C. B. Murray, J. R. Lukes, and M. Drndić, Nano Lett. **14**, 5358 (2014).
[44]W. H. Coulter, U.S. patent 2656508 (October 20, 1953).
[45]S. A. Benner, Astrobiology **17**, 840 (2017).
[46]A. F. Davila and C. P. McKay, Astrobiology **14**, 534 (2014).
[47]F. Rezzonico, Astrobiology **14**, 344 (2014).
[48]K. F. Bywaters, C. P. McKay, A. F. Davila, and R. C. Quinn, in Proceedings of Conference on Biosignature Preservation and Detection in Mars Analog Environments, Lake Tahoe, NV, 16–18 May 2016, paper 2014.
[49]S. S. Johnson, E. Zaikova, D. S. Goerlitz, Y. Bai, and S. W. Tighe, J. Biomol. Tech. **28**, 2 (2017).
[50]A. Mojarro, J. Hachey, R. Bailey, M. Brown, R. Doebler, G. Ruvkun, M. T. Zuber, and C. E. Carr, Astrobiology **19**, 1139 (2019).
[51]S. L. Castro-Wallace, C. Y. Chiu, K. K. John, S. E. Stahl, K. H. Rubins, A. B. R. McIntyre, J. P. Dworkin, M. L. Lupisella, D. J. Smith, D. J. Botkin, T. A. Stephenson, S. Juul, D. J. Turner, F. Izquierdo, S. Federman, D. Stryke, S. Somasekar, N. Alexander, G. Yu, C. E. Mason, and A. S. Burton, Sci. Rep. **7**, 18022 (2017).
[52]K. B. Bywaters, H. J. Schmidt, W. Vercoutere, D. Deamer, A. R. Hawkins, R. C. Quinn, A. S. Burton, and C. P. McKay, ECS Meet. Abstr. **MA2019-02**, 2467 (2019).
[53]W. D. Williams, Mar. Freshwater Res. **37**, 177 (1986).
[54]D. R. Kester, I. W. Duedall, D. N. Connors, and R. M. Pytkowicz, Limnol. Oceanogr. **12**, 176 (1967).
[55]W.-H. Chuang, T. Luger, R. K. Fettig, and R. Ghodssi, J. Microelectromech. Syst. **13**, 870 (2004).
[56]I. Chakraborty, W. C. Tang, D. P. Bame, and T. K. Tang, Sens. Actuators, A **83**, 188 (2000).
[57]J. J. Bock, J. Glenn, S. M. Grannan, K. D. Irwin, A. E. Lange, H. G. LeDuc, and A. D. Turner, Proc. SPIE **3357**, 297–304 (1998).
[58]L. C. Martin, J. D. Wrbanek, and G. C. Fralick, in *ICIASF 2001 Record of 19th International Congress Instrumentation in Aerospace Simulation Facilities (Cat. No.01CH37215)* (University of Michigan, 2001), pp. 196–203.
[59]J. A. Rodríguez-Manzo, M. Puster, A. Nicolaï, V. Meunier, and M. Drndić, ACS Nano **9**, 6555 (2015).
[60]M. D. Fischbein and M. Drndić, Nano Lett. **7**, 1329 (2007).
[61]C.-C. C. Chien, S. Shekar, D. J. Niedzwiecki, K. L. Shepard, and M. Drndić, ACS Nano **13**, 010545 (2019).
[62]M. Waugh, K. Briggs, D. Gunn, M. Gibeault, S. King, Q. Ingram, A. M. Jimenez, S. Berryman, D. Lomovtsev, L. Andrzejewski, and V. Tabard-Cossa, Nat. Protoc. **15**, 122 (2020).
[63]G. Danda, P. Masih Das, Y.-C. Chou, J. T. Mlack, W. M. Parkin, C. H. Naylor, K. Fujisawa, T. Zhang, L. B. Fulton, M. Terrones, A. T. C. Johnson, and M. Drndić, ACS Nano **11**, 1937 (2017).
[64]G. Danda, P. Masih Das, and M. Drndić, 2D Mater. **5**, 035011 (2018).
[65]T. Gilboa, E. Zvuloni, A. Zrehen, A. H. Squires, and A. Meller, Adv. Funct. Mater. (published online).
[66]H. Yamazaki, R. Hu, Q. Zhao, and M. Wanunu, ACS Nano **12**, 012472 (2018).
[67]C. L. C. Ip, M. Loose, J. R. Tyson, M. de Cesare, B. L. Brown, M. Jain, R. M. Leggett, D. A. Eccles, V. Zalunin, J. M. Urban, P. Piazza, R. J. Bowden, B. Paten, S. Mwaigwisya, E. M. Batty, J. T. Simpson, T. P. Snutch, E. Birney, D. Buck, S. Goodwin, H. J. Jansen, J. O'Grady, H. E. Olsen, and MinION Analysis and Reference Consortium, F1000Research **4**, 1075 (2015).
[68]A. K. Wright and M. R. Thompson, Biophys. J. **15**, 137 (1975).

Published under license by AIP Publishing